Dense cores in the dark cloud complex LDN 1188

E. Verebélyi [1,*], **V. Könyves** [2,3], **S. Nikolić** [4], **Cs. Kiss** [1], **A. Moór** [1], **P. Ábrahám** [1], and **M. Kun** [1]

[1] Konkoly Observatory, Research Centre for Astronomy and Earth Sciences, Hungarian Academy of Sciences, Konkoly Thege 15-17, H-1121 Budapest, Hungary

[2] Laboratoire AIM, CEA/DSM-CNRS-Université Paris Diderot, IRFU/Service d'Astrophysique, CEA Saclay, 91191 Gif-sur-Yvette, France

[3] Institut d'Astrophysique Spatiale, UMR8617, CNRS/Université Paris-Sud 11, 91405 Orsay, France

[4] Department of Astronomy, University of Chile, Casilla 36-D, Santiago, Chile

We present a molecular line emission study of the LDN 1188 dark cloud complex located in Cepheus. In this work we focused on the densest parts of the cloud and on the close neighbourhood of infrared point sources. We made ammonia mapping with the Effelsberg 100-m radio telescope and identified 3 dense cores. CS(1–0), CS(2–1) and HCO⁺(1–0) measurements performed with the Onsala 20 m telescope revealed the distribution of dense molecular material. The molecular line measurements were supplemented by mapping the dust emission at 1.2 mm in some selected directions using the IRAM 30 m telescope. With these data we could work out a likely evolutionary sequence in this dark cloud complex.

1 Introduction

LDN 1188 is a star-forming dark cloud complex in the Cepheus region. It is likely associated with the nearby S 140/LDN 1204 region and hence situated at a distance of ∼910 pc according to Ábrahám et al. (1995; hereafter A95). Using CO emission line data A95 identified six ^{13}CO clumps and derived their physical parameters including excitation temperature, H_2 column density and molecular mass. Emission line surveys in this region revealed the presence of Hα emission stars (A95; Drew et al. 2005). In this paper we present the results of our molecular line studies that focused on some selected molecules and transitions and were performed mainly in the direction of previously detected molecular cores or infrared point sources. A comprehensive study of the infrared point sources and young stellar objects identified in the cloud complex is presented in a parallel paper (Marton, Verebélyi & Kiss 2013, this issue).

2 Observations

2.1 NH₃, Effelsberg 100 m

Simultaneous observations of the NH₃ (1,1) and (2,2) rotation-inversion transitions have been carried out with the 100-m radio telescope in Effelsberg in April 1995. We used a 1024 channel autocorrelator as a backend, splitted into two 6.25 MHz bands, centered on the (1,1) and (2,2) frequencies. The system temperature was ∼150 K. Pointing

	Effelsberg	Onsala 1	Onsala 2
Frequency (GHz)	24	90	40
HPBW (arcsec)	40″	45″	80″
Spectral res. (km s^{-1})	0.15	0.04	0.07
Pointing unc. (arcsec)	10	3	3
Main beam eff.	0.3	0.5	0.5
Observational mode	position switch	frequency switch	dual beam switch

Table 1 Key parameters of the observations. Additional information can be found in Section 2.

was checked periodically, by continuum observations of the source W3OH at 23.7 GHz. Table 1 contains the most important parameters of the observation.

The integration times were typically 3 – 5 minutes. Data reduction of the NH₃ data was carried out by the CLASS software (Pety 2005). We fitted Gaussian line profiles and linear baselines in all cases. The resulting map of the LDN 1188 complex consists of some 315 observed positions (see Fig 1), with a beam (cores) or double-beam spacing (outskirts).

2.2 CS and HCO⁺, Onsala 20 m

We used the Onsala Space Observatory (OSO) 20-m telescope over two observational sessions. In the first session, in April/May 2004 (Onsala 1 in Table 1) we made small CS(2–1) maps around five detected ^{13}CO-clumps of A95 and a pointed HCO⁺(1–0) spectrum towards the center of each map. The receiver was a SIS mixer with a typical temperature of $T_{rec} = 80$–110 K. The pointing was checked by

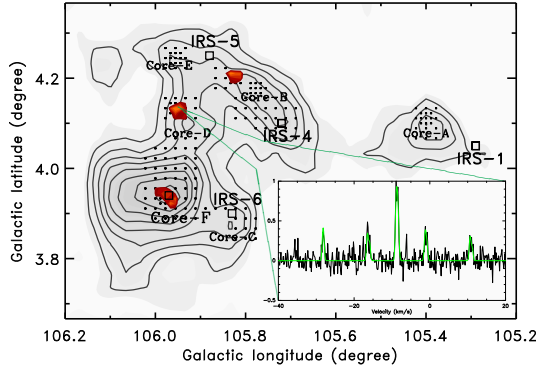⋆ Corresponding author: e-mail: verebelyi.erika@csfk.mta.hu

Fig. 1 Position of the ammonia cores in LDN 1188. Ammonia cores in this figure are shown by small, (red in the online version) shaded areas, where the integrated intensity of the NH_3 (1,1) line exceeded $0.4\,\mathrm{K\,km\,s^{-1}}$ in the velocity interval $-13\,\mathrm{km\,s^{-1}} \leq v_{\mathrm{LSR}} \leq -5\,\mathrm{km\,s^{-1}}$. This corresponds to the $\sim 2\sigma$ noise level of integrated intensity in this region. The light grey filled contours and solid contour lines mark the $^{13}\mathrm{CO}$ integrated intensity contours, from $2\,\mathrm{K\,km\,s^{-1}}$ with $1\,\mathrm{K\,km\,s^{-1}}$ increment, as in Figs. 3 and 6 of A95; black dots indicate the positions of ammonia observations. IRAS sources are marked with squares. In the inserted subfigure we present a sample NH_3 spectrum that corresponds to the peak emission in Core D. The solid black line is the measured intensity, the green curve is the fitted profile.

observing the SiO maser sources IK Tau and R Cas. In the second observational period (in July 2005, Onsala 2 in Table 1) CS(1–0) observations were performed. Three of the five cores were mapped in the lower CS transition and towards the remaining two cores we made pointed observations. The receiver was a HEMT with a typical $T_{\mathrm{rec}} = 50\,\mathrm{K}$. We used a 1600-channel correlator with a 20 MHz bandwidth. In both cases the chopper-wheel method was used for calibration, and the intensity scale is given in terms of T_{A}^*. We used a grid spacing of $30''$ for the CS(2–1) maps and of $40''$ for the CS(1–0) maps (see also Table 1).

2.3 IRAM 30 m, 1.2 mm continuum

Three areas (centered at the infrared sources IRS 4, 5 and 6; see A95) were observed with the MAMBO-II bolometer array on the IRAM 30m telescope on December 14, 2003, using on-the-fly mapping mode with $42''$ wobbler throw and 0.5 Hz wobbler period. Our calibrators were NGC 7538, Cep A, HL Tau and Ori A–IRS 2. Pointing accuracy was measured to be better than $9.5''$ while the HPBW was $11''$. The data were reduced using MOPSIC[1], the upgraded version of MOPSI (Zylka 1998). The measured flux densities were corrected for variations of telescope gain and converted into Jansky units using the table provided by R. Cesaroni (priv. com.).

[1] http://www.astro.rurh-uni-bochum.de/nielbock/simba/mopsic.pdf

Core	l	b	τ	T_{ex}	T_{kin}	N(1,1)	N(NH$_3$)
	[°]	[°]		[K]	[K]	[10^{14} cm^{-2}]	[10^{14} cm^{-2}]
B	105.81	4.20	0.5±0.3	12.1	14.9	1.6±0.9	4.4±2.7
D	105.96	4.13	1.9±0.5	12.2	15.0	3.5±1.0	9.3±3.0
F	105.98	3.93	0.3±0.2	11.9	14.6	1.0±0.7	2.7±2.0

Table 2 Main parameters from NH_3 emission at the three cores (Fig. 1.) where the signal-to-noise ratio was higher than 2. The columns are: (1) Name of the cores, (2, 3) Galactic coordinates, (4) Optical depth from the main group of the observed (1,1) transition line, (5) T_{ex} excitation temperature, (6) T_{kin} kinetic temperature, (7) the (1,1) level population number, (8) NH_3 column density.

3 Dense cores in LDN 1188

3.1 Ammonia cores

We found three separated ammonia cores, defined as regions above $0.4\,\mathrm{km\,s^{-1}}$ integrated intensity in the velocity interval of -13 $\mathrm{km\,s^{-1}} < v_{\mathrm{LSR}} <$ -5 $\mathrm{km\,s^{-1}}$. These cores coincide with the CO clumps B, D and F, both in position and velocity, however, in some cases they are slightly offset from the $^{13}\mathrm{CO}$ core centers. The size of the ammonia cores are in the order of $\sim 1'$. The location of the ammonia cores are shown in Fig. 1, together with the $^{13}\mathrm{CO}$ integrated intensity contours of A95. The peak integrated intensities are 0.85, 0.87 and 0.65, with r.m.s. uncertainty of 0.13 K km s^{-1} (around the peaks), in the Core B, D and F, respectively.

In molecular clouds, the rotation–inversion transitions of NH_3 are excited in collisions, mainly with H_2, and their relative intensities indicate the kinetic temperature of the gas. Line optical depths of the main components of the (1,1) and (2,2) transitions, excitation and kinetic temperature and the total column density of ammonia were derived following the procedures described in Mangum, Wootten & Mundy (1992) (Eq. 1) and Rohlfs & Wilson (2004) (Eq. 2), assuming local thermodynamic equilbrium (LTE). Because of the low detection level of (2,2) transiton line, a non-LTE excitation model could not be applied.

$$N(1,1) = 6.60 \cdot 10^{14} \cdot \frac{T_{\mathrm{ex}}}{\nu(1,1)} \cdot \tau(1,1,m) \cdot \Delta v \qquad (1)$$

$$N(NH_3) = N(1,1) \cdot \left[\frac{1}{3} e^{\frac{23.1}{T_{\mathrm{kin}}}} + 1 + \frac{5}{3} e^{\frac{-41.2}{T_{\mathrm{kin}}}} + \frac{14}{3} e^{\frac{-99.4}{T_{\mathrm{kin}}}} \right] \qquad (2)$$

Physical properties were derived in three positions (Core B, D and F), where the signal-to-noise ratio was higher than 4 σ in all cases, as listed in Table 2. The main uncertainty of the calculated column densities originates from the error of the optical depth, $\tau(1,1,m)$. The T_{kin} values were used to define the temperature in the CS model later.

3.2 CS and HCO+ lines

While the ammonia measurements covered the whole area of the $^{13}\mathrm{CO}$ contours shown in Fig. 1, the center of CS and

Table 3 Observed parameters of the molecular cores in the LDN 1188 complex. The table lists the main beam temperatures or antenna temperatures, central velocities and velocity dispersions for each line observed. For the ammonia transitions only the main component parameters are given. The asterisk (*) marks the 2σ detection, while (†) gives the upper limit of the intensity i.e., the 1σ value.

Source	CS (1–0)			CS (2–1)			HCO$^+$(1–0)			NH$_3$ (1,1)			NH$_3$ (2,2)		
	T_{mb}	v_{LSR}	Δv	T_{mb}	v_{LSR}	Δv	T_{mb}	v_{LSR}	Δv	$T_{\mathrm{A*}}$	v_{LSR}	Δv	$T_{\mathrm{A*}}$	v_{LSR}	Δv
	[K]	[km/s]	[km/s]	[K]	[km/s]	[km/s]	[K]	[km/s]	[km/s]	[K]	[km/s]	[km/s]	[K]	[km/s]	[km/s]
IRS 1	0.26*	−10.38	0.88	0.19*	−10.38	1.10	1.04	−10.42	1.29	0.13†			0.13†		
IRS 4	0.82	−10.77	1.12	0.78	−10.47	2.04	0.44*	−10.03	1.58	0.21	−9.96	1.56	0.12†		
IRS 5	0.60*	−9.16	0.90	0.17*	−8.93	1.58	0.60†			0.10†			0.13†		
IRS 6	1.52	−9.13	0.70	0.61	−9.14	1.11	1.74	−9.05	0.86	0.18*	−11.27	1.18	0.07†		
Core-F	2.24	−8.83	1.02	1.28	−8.72	1.31	0.50*	−8.90	1.20	0.41	−8.69	1.02	0.22*	−8.50	0.26

HCO$^+$ observations are indicated with squares. These coincide with IRAS point sources found in the cloud (see A95) except the case of Core–F which is starless, the most massive ($\sim 1000\,M_\odot$, A95), although not the largest. Table 3 gives the Gaussian fits to the observed lines of the cores, with the CS(2–1) line convolved to the CS(1–0) line's spatial resolution.

To estimate some physical properties of the dense molecular gas we applied the non–LTE excitation and radiative transfer code, RADEX (Van der Tak et al. 2007) on our CS line emission data. The model uses the mean escape probability approximation (MEP) for radiative transfer equations, effectively decoupling radiation from molecular excitation. RADEX includes collisions, spontaneous and stimulated radiative transitions and computes statistical equilibrium for rotation levels of an interstellar molecule and predicts line brightness temperatures. In this model clouds are assumed to be spherical, homogeneous, isothermal, with constant density and abundances.

The values of the parameters (kinetic temperature, CS column densities, hydrogen molecule number density) were varied in the range of $T_{\mathrm{kin}} = 5 - 25$ K, $N(\mathrm{CS}) = 10^{11} - 10^{16}\,\mathrm{cm}^{-2}$, $n(\mathrm{H_2}) = 10^3 - 10^8\,\mathrm{cm}^{-3}$. The χ^2 was computed using the ratio $\mathcal{R} = \mathrm{CS(2–1)/CS(1–0)}$ i.e., $\chi^2 = (\mathcal{R}_{mod} - \mathcal{R}_{obs}) \cdot \Delta\mathcal{R}_{obs}^{-2}$, where 'mod' and 'obs' are the modelled and the observed ratios, and the errors in the line intensities are the Gaussian fit errors. To make the comparison possible the CS (2–1) spatial resolution was convolved (degraded) to the CS (1–0) resolution. The final solutions were restricted by three times the minimum χ^2 value and by a surface beam filling factor < 1, which were defined as $T_{\mathrm{obs}}/T_{\mathrm{mod}}$ for the CS (1–0) transition.

In Table 4 we present the model results for the best fit hydrogen number density estimate of $5 \times 10^4\,\mathrm{cm}^{-3}$. The size of the cores was derived as a geometrical mean of the half maxima of the CS (2–1) integrated intensity. To calculate the molecular hydrogen column density we assumed an average relative CS abundance of $\approx 2 \times 10^{-9}$ found in LDN 1251 (Nikolić, Johansson & Harju 2003) to be valid here as well. The adoption of this value can be justified by the location of both clouds/complexes in the Cepheus region and also by the presence of cores in all evolutionary stages,

from starless cores to those that harbour Class I YSOs. For the core mass calculation we assumed that the cores are homogeneous and that the surface and volume filling factors are the same. The derived masses are corrected for the presence of He.

3.3   The 1.2 millimetre cores

Table 5 gives the center positions and derived flux densities of the IRAS sources observed with IRAM bolometer array. We defined a source as a compact region with a local maximum of intensity in the 1.2 mm maps, which is separated from the background and/or from other sources by at least 2σ backgrund uncertainty contours. Both IRS 4 and IRS 6 could be resolved into multiple sources. The flux density of the sources was derived by aperture photometry. The local background level and background r.m.s. noise were derived in a nearby, apparently unobscured region. Figure 2 gives the IRAM 1.2 mm continuum emission for IRS 4 and IRS 6. In the case of IRS 5 the detected emission was too weak and quite extended to identify any compact source, therefore the value given in Table 5 should be considered as an upper limit.

Table 4 Physical parameters derived from millimetre line observations, the best fit model is for the molecular hydrogen density of $5 \times 10^4\,\mathrm{cm}^{-3}$. Columns: (1) source-name, (2) kinetic temperature estimated from the ratio of CS lines, (3) calculated CS column density, (4) beam surface filling factor from the observed and modelled line intensity ratio, (5) radius of the CS-core, (6) total mass of the cores.

Source	T_{kin}	$N(\mathrm{CS})$	ff	r	M
	[K]	[$10^{13}\,\mathrm{cm}^{-2}$]	[%]	[pc]	[$\mathrm{M_\odot}$]
IRS 1	13 ± 5	0.2 ± 0.1	20	0.12	0.4
IRS 4	16 ± 4	1.2 ± 0.3	30	0.23	12.9
IRS 5	16 ± 2	0.3 ± 0.1	20	0.10	0.4
IRS 6	10 ± 5	1.6 ± 0.9	40	0.27	31.5
Core-F	8 ± 2	3.2 ± 0.8	70	0.29	127.3

Source	Flux density (mJy)	Galactic coordinates (deg, deg)
IRS 4–1	63±18	105.7279 +4.1061
IRS 4–2	42±14	105.7273 +4.1013
IRS 5	<63	105.8724 +4.2469
IRS 6–1	149±20	105.8330 +3.9003
IRS 6–2	102±16	105.8278 +3.9032
IRS 6–3	73±15	105.8245 +3.9015

Table 5 Derived flux densities and coordinates of the sources identified with IRAM bolometer in IRS 4, 5 and 6. Note that the flux density of IRS 5 is an upper limit and that the absolute pointing accuracy was $9''\!.5$ ($0°\!.0026$).

4 Discussion

The NH_3 column densities determined in this work for LDN 1188 are typical for dark clouds/cores in this area. In the cores of LDN 1251 and LDN 1204/S 140 the column densities are similar to those in the LDN 1188. However, the kinetic temperatures are 2–5 K lower than in the case of LDN 1251, and equal to or slightly higher than in LDN 1204 (Tóth & Walmsley 1996; Jijina, Myers & Adams 1999, respectively). We also compared the dense core masses (traced by CS as derived in this paper) and those masses that were derived from the CO measurements by A95 for each core. Meaningful values could be derived
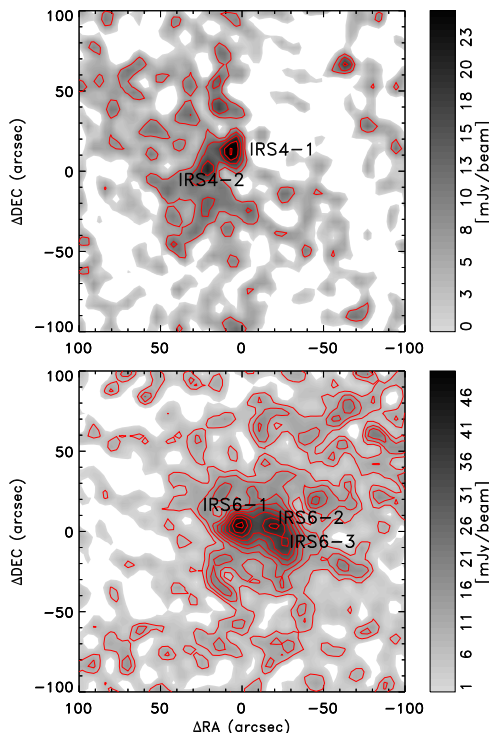

Fig. 2 The IRAM bolometer maps of IRS 4 (top) and IRS 6 (bottom panel). Intensity-contours are drawn from 7.5 by 5 mJy/beam, the coordinates are relative w.r.t the map centre.

for three cores and we obtained 5, 21 and 13 per cent for IRS 4, IRS 6 and Core-F, respectively, indicating that the molecular material is most concentrated in IRS 6. In IRS 1 and IRS 5 the molecular lines are weak, the CS column densities and filling factors are very low and IRS 5 is not clearly observable at 1.2 mm. This indicates that molecular material is not dominant and that these regions are likely in a more advanced evolutionary state. Using the observed velocity dispersion and size of the cores we could estimate the dynamical timescales which are in the range of $1–5 × 10^5$ yr, similar to that found by Tóth & Walmsley (1996) in the LDN 1251.

5 Summary

We have carried out NH_3 spectral-line observations within the ^{13}CO-contour of the LDN 1188 molecular cloud complex presented in A95. We identified ammonia cores in three of the previously known six CO-clumps. These ammonia cores are probably the densest parts of the cloud, and clearly seen to be far from the detected IRAS point sorces (A95; Könyves et al. 2004). Star formation is likely still ongoing in these cores. Additional molecular line (CS and HCO^+) observations show that most molecular material is located in the starless core Core-F, but still significant amounts of matter exist around IRS 4 and IRS 6. The IRS 1 and IRS 5 sources are likely in a more advanced evolutionary stage since the amount of molecular material is notably lower in the vicinity of these source.

References

Ábrahám, P., Dobashi, K., Mizuno, A. et al.: 1995, A&A 300, 525
Drew, J. E., Greimel, R., Irwin, M. J. et al.: 2005, MNRAS 362, 753
Jijina, J., Myers, P. C. & Adams, F. C.: 1999, ApJS 125, 161
Könyves, V., Moór, A., Kiss, Cs. et al.: 2004, BaltA 13, 470
Mangum, J. G., Wootten, A. & Mundy, L. G.: 1992, ApJ 388, 467
Marton, G., Verebélyi, E. & Kiss, Cs.: 2013, AN this issue
Nikolić, S., Johansson, L. E. B. & Harju, J.: 2003, A&A 409, 941

Pety, J.: 2005, Semaine de l'Astrophysique Francaise, ed. F. Casoli
    et al., EDP Sciences, p. 721
Rohlfs, K. & Wilson, T. L.: 2004, Tools of Radio Astronomy,
    Springer-Verlag
Van der Tak, F. F. S., Black, J. H., Schier, F. L. et al.: 2007, A&A
    468, 627
Tóth, L. V. & Walmsley, C. M.: 1996, A&A 311, 981
Zylka, R., 1998 The MOPSI Cookbook (Bonn, MPIfR),
    http://www.mpifr-bonn.mpg.de/staff/bertoldi/mambo/